

# Effect of a Self-Assembled Nucleating Agent on the Crystallization Behavior and Spherulitic Morphology of Poly(lactic acid)

Zhixiang Yan, Yanqin Huang, Wenfeng Zhao, Bin Wu, Chengkai Liu, Xiangyu Yan, Hongwei Pan, Yan Zhao,\* and Huiliang Zhang



Cite This: *ACS Omega* 2023, 8, 44093–44105



Read Online

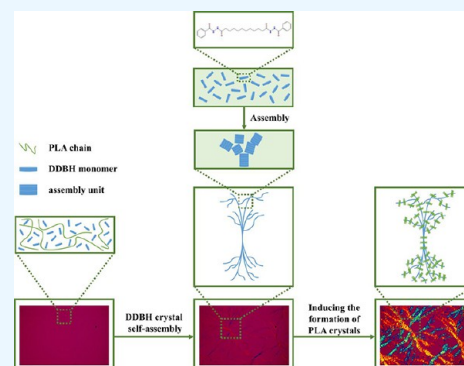
ACCESS |

Metrics & More

Article Recommendations

Supporting Information

**ABSTRACT:** Herein, decanedioic acid dibenzoylhydrazide (DDBH) was used as a nucleating agent to improve the crystallization of poly(lactic acid) (PLA). The formation of DDBH assemblies in PLA melts at different concentrations was systematically investigated. The DDBH (0.5–0.9 wt %) recrystallized as dendrite-like structures during the isothermal crystallization process, and the crystal morphology of PLA underwent a morphological change from spherical form to a similar dendritic crystal form. Differential scanning calorimetry and in situ wide-angle X-ray diffraction analysis results showed that crystallizability and overall crystallization rate of PLA were enhanced by the addition of DDBH. The half-crystallization time at 120 °C reduced to 0.28 min compared to pure PLA (6.12 min), after adding 0.9 wt % DDBH. Moreover, the crystallinity and lamellar thickness of crystalline PLA increased, while the size of the microcrystal of PLA decreased with an increase in DDBH content. The heat deflection temperatures of PLA/DDBH blends increased and hence heat resistance improved.



## 1. INTRODUCTION

In the last several decades, rapid developments and widespread applications of polymer materials have led to a serious problem of environmental pollution.<sup>1,2</sup> To solve this problem, traditional petroleum-based polymers have been substituted with biodegradable polymers to reduce plastic wastes.<sup>3–5</sup> For example, poly(lactic acid) (PLA), a popular biodegradable polymer derived from renewable plant resources, possessing good biocompatibility and high mechanical strength, has received great attention from researchers.<sup>6–8</sup> However, PLA has a relatively low crystallization rate and low heat distortion temperature, which has limited its further application.<sup>9,10</sup> PLA, a semicrystalline polymer, whose crystallization is interesting since it affects many intrinsic properties.<sup>11</sup> Because of its slow crystallization rate and long crystallization time, PLA is inefficient in actual processes of extrusion and blow molding.<sup>12,13</sup> Moreover, the low crystallinity of PLA results in low heat distortion temperature and poor dimensional stability, which causes thermal deformation when heated.<sup>14,15</sup>

Introduction of nucleating agents (NAs) is one of the most practical strategies to control the crystallinity of PLA during processing.<sup>15</sup> NA provides numerous nucleating sites for polymer crystallization and reduces the surface free energy barrier for nucleation, which significantly accelerates the crystallization and increases the crystallization temperature of PLA.<sup>16,17</sup> There are three types of NAs usually used to control the crystallinity of PLA: inorganic NA, organic NA, and macromolecular NA. Inorganic NAs, such as calcium

carbonate,<sup>18</sup> silica,<sup>19</sup> montmorillonite,<sup>20</sup> talc,<sup>21</sup> boron nitride nanotubes,<sup>22</sup> and  $Ti_3C_2T_x$  MXene<sup>23</sup> have abundant resources and are low in cost. However, due to the poor compatibility between inorganic NA and PLA matrix, the incorporation of inorganic NA usually reduces the mechanical properties of PLA. Organic NAs, such as hydrazides,<sup>24,25</sup> amides,<sup>26,27</sup> and organic acid salts,<sup>28–30</sup> have better miscibility in PLA, and can significantly promote the crystallization of PLA. Macromolecular NAs, such as nanocrystalline cellulose,<sup>31</sup> cyclodextrin,<sup>32</sup> poly(D-lactic acid),<sup>33</sup> and poly(glycolic acid),<sup>34</sup> have been commonly used for research studies but are not suitable for the manufacturing of PLA products. Among these NAs, hydrazide is one of the most important and effective NAs for PLA, which mainly includes decanedioic acid dibenzoylhydrazide (DDBH)<sup>24</sup> and hexanedioic acid dibenzoylhydrazide (HDBH).<sup>25</sup>

In actual processing, NAs usually show different structures from the original forms in PLA melts.<sup>35,36</sup> In the case of insoluble NAs, the NAs disperse in PLA and then aggregate together to induce the crystallization of PLA.<sup>26,37</sup> In the case of soluble NAs, the NA dissolves in the PLA during the heating

**Received:** August 27, 2023

**Revised:** October 24, 2023

**Accepted:** October 26, 2023

**Published:** November 6, 2023



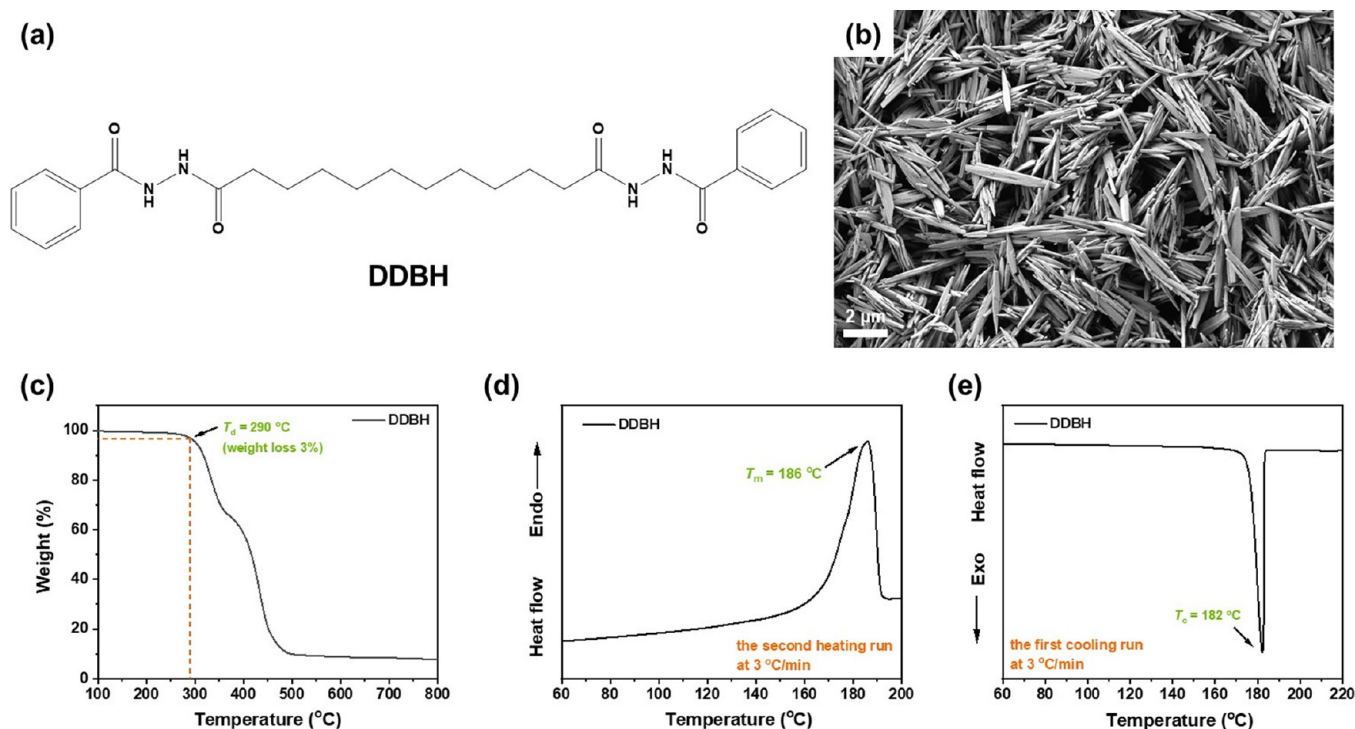


**Figure 1.** Structure of DDBH (a), SEM micrographs of DDBH (b), TGA curves of DDBH (c), and DSC curves of DDBH (d and e).

process, after which the dissolved NAs would recrystallize into different structures, thus demonstrating their different nucleating effects.<sup>24,25</sup> The real structure of NA that induces PLA crystallization is often different from its original form and is determined from its dispersion state during heating and its recrystallization behavior during cooling. Therefore, the structural evolution and final recrystallization structure of NA in PLA under different experimental conditions were studied.

In this work, DDBH was used as the NA to enhance the crystallization behavior of PLA. The structural evolution of different concentrations of DDBH in PLA melts was studied. Moreover, the effect of DDBH on the crystal morphology of PLA was studied by polarizing optical microscopy. Based on the results of differential scanning calorimetry (DSC) and in situ wide-angle X-ray diffraction (WAXD) analysis, the effects of DDBH on the nonisothermal melt crystallization and overall isothermal crystallization behaviors of PLA/DDBH blend were investigated. Considering the fact that crystallinity is closely associated with heat resistance, WAXD and small-angle X-ray scattering (SAXS) analyses were conducted to study the effect of DDBH on the degree of crystallinity, the apparent crystal size, and crystalline lamellar thickness of PLA. This study presents some fundamental understanding of the structural evolution of the PLA/DDBH blend and helps to establish the exact relationship between its crystalline structures and performance.

## 2. MATERIALS AND METHODS

**2.1. Materials.** PLA (4032D,  $M_w$  190,000 g/mol, PDI: 1.41, D-isomer: 2.0 wt %) was purchased from NatureWorks Co. Ltd. (USA). DDBH was bought from Nanjing Baitong New Material Co. Ltd. The structure and SEM images of DDBH are shown in Figure 1a,b. The initial decomposition temperature ( $T_d$ , Figure 1c) and melting temperature ( $T_m$ ,

Figure 1d) of DDBH were determined as 290 and 186 °C, respectively.

**2.2. Preparation of PLA/DDBH Blends.** The PLA pellets were dried in a vacuum oven at 60 °C for 24 h. The PLA/DDBH blends were melt blended in a mixer at a rotating speed of 65 rpm and 200 °C for 5 min. The obtained blends were subjected to hot pressing at 200 °C for 5 min and then compression molded at 25 °C for 5 min. The components of the blends are presented in Tables 1 and S1.

**Table 1. Components of PLA and PLA/DDBH Blends**

samples	PLA (wt %)	DDBH (wt %)
pure PLA	100	0
PLA/DDBH-0.1	99.9	0.1
PLA/DDBH-0.3	99.7	0.3
PLA/DDBH-0.5	99.5	0.5
PLA/DDBH-0.7	99.3	0.7
PLA/DDBH-0.9	99.1	0.9

**2.3. Characterization.** **2.3.1. Polarized Optical Microscopy.** Spherulitic growth of samples was monitored by a polarized optical microscope (POM, Axio Scope, Zeiss, Germany), equipped with a hot stage (THMS 600, Linkam, UK). During nonisothermal crystallization process, samples were heated to 200 °C and held at 200 °C for 5 min for the elimination of any thermal history. Then, the samples were cooled to 50 °C at a rate of 5 °C/min.

In the isothermal crystallization process, samples were first heated at 200 °C for 5 min and then cooled to 130 °C at 30 °C/min using liquid nitrogen. And then the samples were conducted at 130 °C for 60 min.

**2.3.2. Rheological Properties.** Rheological testing of the samples was conducted with a rotational rheometer (MCR301, Anton Paar, Austria). The frequency for the dynamic

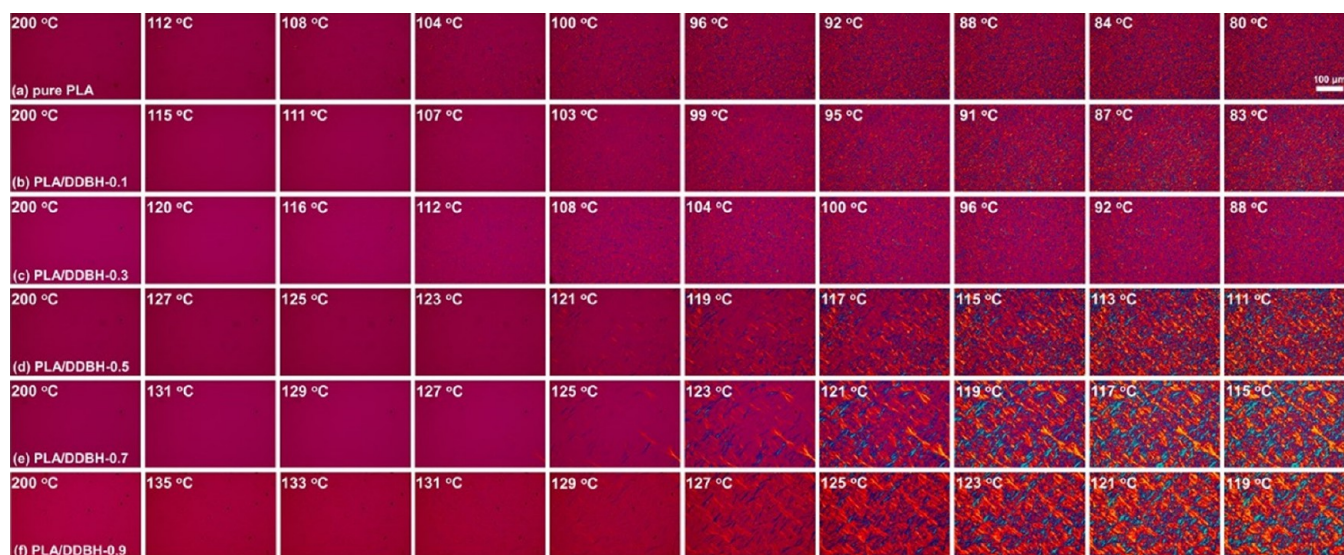


**Figure 2.** POM micrographs of pure PLA and PLA/DDBH blends cooled from 200 °C (scale bar is 100  $\mu\text{m}$ ).

temperature sweep runs was 1 Hz and the strain was set to 1%. The samples were heated at 200 °C for 5 min and then cooled to 100 °C at 3 °C/min.

The frequency range for the dynamic frequency sweep tests was 0.1–100 rad/s, and the strain value was set to 1% in the linear viscoelastic region. The testing was carried out at 200 °C.

**2.3.3. Differential Scanning Calorimetry.** Thermal properties of the samples were tested using DSC (Mettler, Switzerland). In the nonisothermal crystallization process, samples were heated to 200 °C and held at 200 °C for 5 min. Then, the samples were cooled to 0 °C at 10 °C/min. After cooling, the samples were reheated to 200 °C at 10 °C/min.

In the isothermal crystallization process, samples were heated from 0 to 200 °C at 30 °C/min and then held at 200 °C for 5 min. Then, the samples were cooled to the crystallization temperature ( $T_c$ ) at 30 °C/min and held at  $T_c$  until the isothermal crystallization was complete.  $T_c$ s were set at 120, 115, and 110 °C.

The self-nucleation experiment was according to a method reported by Wittmann et al.<sup>38</sup> The procedure was described as follows: (1) neat PLA was first heated to 200 °C at a rate of 30 °C/min and held at 200 °C for 5 min to eliminate the thermal history. Then, the sample was cooled to 80 °C at 5 °C/min to provide a standard thermal history; (2) after cooling, the sample was reheated to a self-nucleation temperature ( $T_s$ ) at 10 °C/min and held for 5 min to create self-nucleated seeds; and (3) the sample was then cooled to 80 °C at 5 °C/min. The crystallization peak temperatures ( $T_c$ ) of the self-nucleated PLA were determined by the DSC cooling curves.

**2.3.4. WAXD Analysis.** WAXD analysis was performed using an X-ray diffractometer (SmartLab, Rigaku, Japan) with a Cu  $K\alpha$  radiation source ( $\lambda = 1.54 \text{ \AA}$ ). The scanning range of the diffraction angle ( $2\theta$ ) was from 10° to 30° at a scanning speed of 2°/min.

In situ WAXD measurements were conducted with an X-ray diffractometer (DX-2700BH, Haoyuan, China). The wavelength of the X-ray beam was 0.154 nm. The scanning was conducted in the range of 10° to 30°, with a step size of 0.05 mm and the scanning speed was 0.5 s/step. The temperature was controlled using a hot stage (HCP621G, Instec, USA).

The samples were heated to 200 °C at 30 °C/min and held at 200 °C for 10 min. Then, the samples were cooled to 50 °C at 5 °C/min. A 1D detector (Mythen2, Dectris, Switzerland) was used to track the changes in crystallinities of the samples by short-distance photography. The exposure time for each sample was set as 12 s.

**2.3.5. SAXS Analysis.** SAXS analysis was performed on an SAXS system (Xeuss 2.0, Xenocs, France) using a Mo  $K\alpha$  radiation source. The wavelength of X-ray of radiation source was 0.134 nm. The diffraction angle ( $2\theta$ ) was 3.4° and the scattering vector ranged from 0.02 to 2.0  $\text{nm}^{-1}$ .

**2.3.6. Fourier Transform Infrared Spectroscopy.** Fourier transform infrared (FT-IR) spectra of pure PLA and PLA/DDBH samples were obtained on an FT-IR spectrometer (IRTracer-100, Shimadzu, Japan) in the attenuated total reflectance mode (ATR). The wavenumber range was 4000–500  $\text{cm}^{-1}$  with a resolution of 4  $\text{cm}^{-1}$  and 128 scans of each sample.

**2.3.7. Heat Deflection Temperature Test.** Heat deflection temperatures (HDT) of pure PLA and PLA/DDBH blends were measured by an HDT tester (WKW-300) in accordance with GB/T 1634.2. Samples were heated from room temperature to their HDTs at 2 °C/min, and the bending stress was 1.80 MPa. The dimensions of the specimen were 70  $\times$  10  $\times$  4 mm.

## 3. RESULTS AND DISCUSSION

**3.1. Crystalline Morphology of Pure PLA and PLA/DDBH Blends.** POM was employed to study the structural changes of DDBH in the PLA (for different concentrations of DDBH from 0 to 0.9 wt %), when cooled from 200 °C at 5 °C/min (Figure 2). It was found that DDBH recrystallized into diverse assemblies at different concentrations under the same thermal conditions. Pure PLA (Figure 2a) showed the presence of some relatively dark small spherulites at 112 °C. As the testing temperature decreased, the number of PLA spherulites increased in number. As shown in Figure 2b,c, no crystals of DDBH were observed during the cooling process in the PLA/DDBH-0.1 and PLA/DDBH-0.3 blends. However, the crystallization temperatures of PLA in the PLA/DDBH-0.1 and PLA/DDBH-0.3 blends increased to 115 and 120 °C,

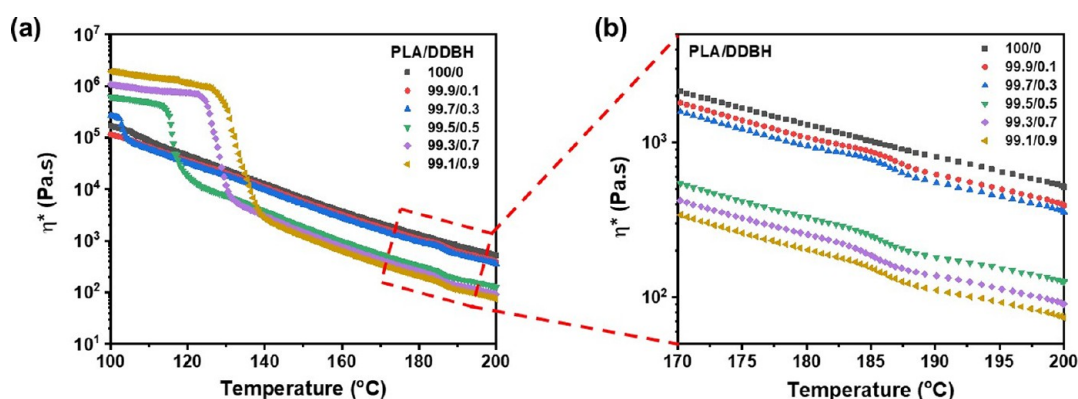


**Figure 3.** (a) Temperature dependence of complex viscosity of pure PLA and PLA/DDBH blends cooled from 200 to 100 °C and (b) partially enlarged curves of pure PLA and PLA/DDBH blends in the range of 170–200 °C.

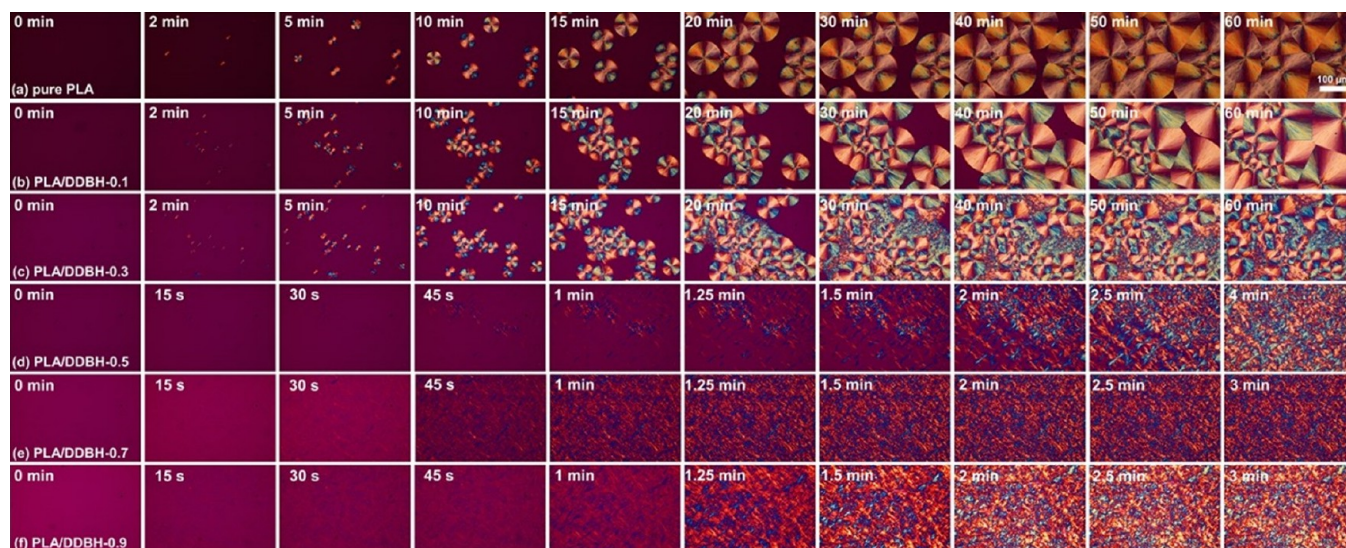


**Figure 4.** POM micrographs of pure PLA and PLA/DDBH blends at a crystallization temperature of 130 °C for different times (scale bar = 100  $\mu\text{m}$ ).

respectively. This suggested that DDBH was already crystallized and formed granules prior to the crystallization of PLA, but the size of the granules was too small to be observed by POM. In the PLA/DDBH-0.5 blend (Figure 2d), DDBH disappeared at 200 °C and recrystallized into dendrite-like structures while cooling, thus enabling PLA to crystallize in the form of dendritic crystals. PLA/DDBH-0.7 and PLA/DDBH-0.9 blends (Figure 2e,f) showed a similar behavior. Interestingly, the structures of dendrites DDBH formed at concentrations of 0.5–0.9 wt % showed varied sizes. With an increase in the concentration of DDBH, the size of dendrites increased. Moreover, the crystallization temperature of PLA enhanced and size of finally formed PLA crystals increased with an increase in DDBH content.

The process of assembly of DDBH and the crystallization process of PLA could be seen in rheological testing. The changes in complex viscosity ( $\eta^*$ ) of pure PLA and its blends on cooling from 200 to 100 °C were shown in Figure 3a. For pure PLA and PLA/DDBH-0.1 samples, the values of  $\lg(\eta^*)$  increased linearly as the temperature decreased. In contrast, when the concentration of DDBH was more than 0.1 wt %, there was a sharp increase in the  $\eta^*$  value between 140 and 100 °C, which corresponded to the crystallization of PLA. It is noteworthy that as the DDBH content increased, the

crystallization temperature of PLA increased gradually. Moreover, as the DDBH concentration increased, the low-temperature  $\eta^*$  values of PLA/DDBH blends increased. The increase in low-temperature  $\eta^*$  of PLA/DDBH blends with an increase in DDBH content could be attributed to the crystallization of PLA, which had a higher modulus and melting point. As DDBH content increased, the amount of PLA crystallized during the cooling process increased. Moreover,  $\eta^*$  of PLA/DDBH blends decreased as the DDBH content increased between 200 and 140 °C. The  $\eta^*$  values for neat PLA and PLA/DDBH blends as functions of angular frequency ( $\omega$ ) were determined (Figure S1). In comparison to pure PLA, the PLA/DDBH blends had lower  $\eta^*$  values. As the DDBH content increased, the  $\eta^*$  values of the PLA/DDBH blends decreased significantly. The DDBH was dispersed evenly in the PLA melt and the effect was somewhat similar to that achieved with the addition of trace amounts of low-molecular-weight plasticizer. It had a plasticizing effect on PLA, which was consistent with the reported literature.<sup>39</sup> Interestingly, the PLA/DDBH blends showed an extra upturn in the  $\eta^*$  values at about 185 °C (Figure 3b). According to Figure 1e, the crystallization temperature ( $T_c$ ) of DDBH was about 182 °C during the first cooling run. The appearance of the viscosity step might be

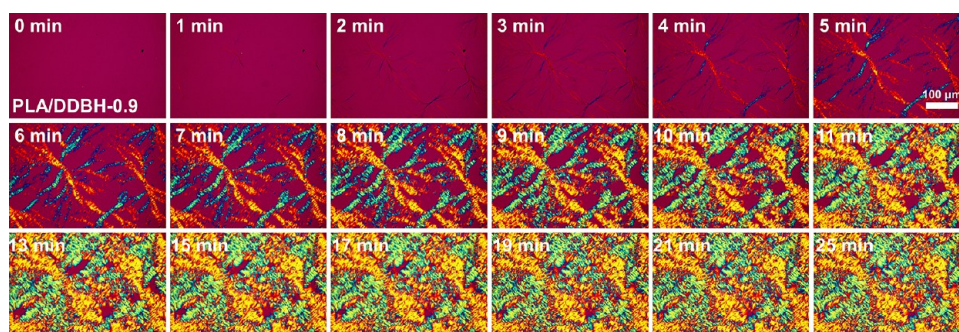


Figure 5. POM micrographs of the PLA/DDBH-0.9 blend at a crystallization temperature of 150 °C for different times (scale bar is 100  $\mu\text{m}$ ).

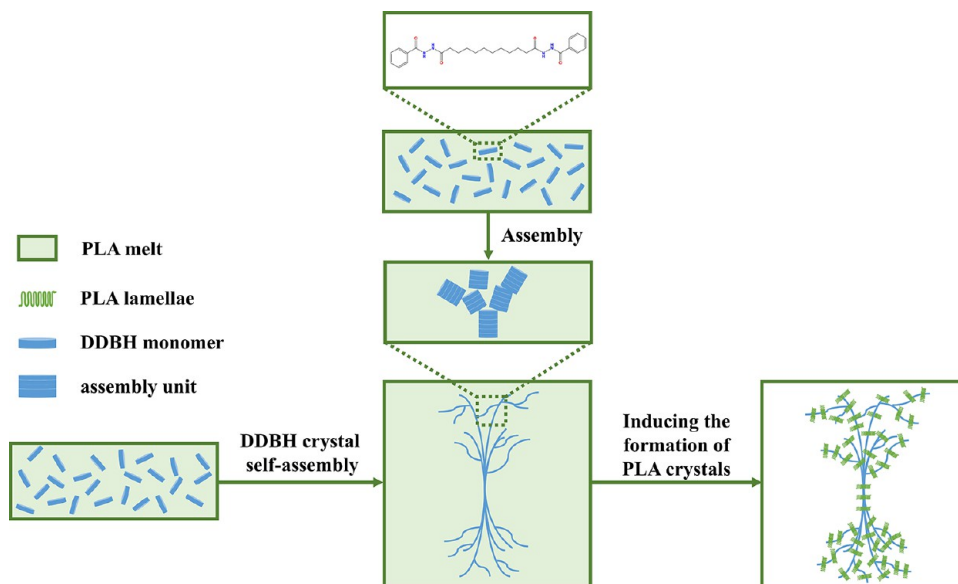


Figure 6. Schematic diagram of the self-assembly process of DDBH and the crystallization process of the PLA/DDBH blend.

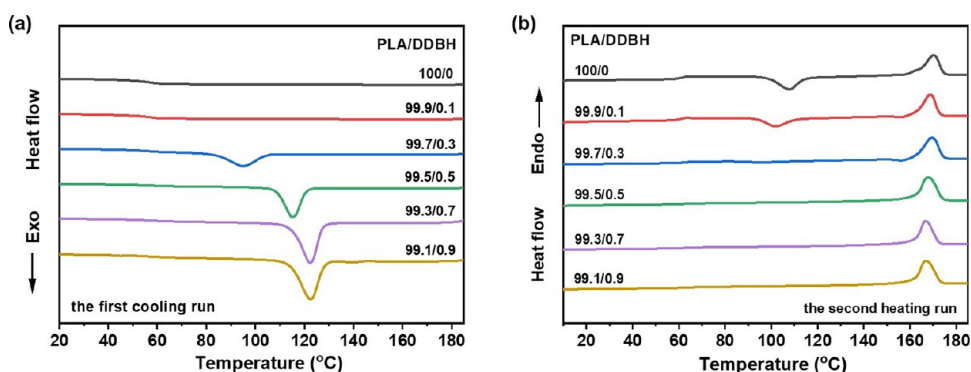


Figure 7. DSC curves of pure PLA and PLA/DDBH blends in the first cooling run (a) and the second heating run at a rate of 10 °C/min (b).

attributed to the crystallization of DDBH.<sup>40,41</sup> On crystallization of DDBH in the PLA melt upon cooling, the reassembly of DDBH resulted in an increase in the  $\eta^*$  values.<sup>36</sup>

The influence of DDBH on crystalline morphologies of PLA during PLA/DDBH blends was studied by POM. The morphological evolutions of pure PLA and PLA/DDBH samples upon cooling to 130 °C for 60 min are shown in Figure 4. The pure PLA crystallized into well-developed spherulites with black extinction crosses after 60 min (Figure 4a). The PLA/DDBH-0.1 blend did not show DDBH crystals under POM during the isothermal crystallization process due

to its low concentration and since PLA crystallized in the form of fine spherulites (Figure 4b). In the case of the PLA/DDBH-0.3 blend (Figure 4c), part of PLA crystallized as the spherulites. Compared to pure PLA, the size of the spherulite crystalline decreased and the number of the spherulites increased. The other part of PLA crystal did not have the shape of spherulite crystalline morphology, instead appeared as a smaller granule with broken crystal shape. This could be ascribed to the reassembly of DDBH into tiny granules, accompanied by an increase in nucleation density of spherulites and a decrease in spherulites size. In the

Table 2. Thermal Properties of Pure PLA and PLA/DDBH Blends

samples	the first cooling run		the second heating run				
	$T_{c,PLA}$ ( $^{\circ}C$ )	$\Delta H_{c,PLA}$ (J/g)	$T_{g,PLA}$ ( $^{\circ}C$ )	$T_{cc,PLA}$ ( $^{\circ}C$ )	$\Delta H_{cc,PLA}$ (J/g)	$T_{m,PLA}$ ( $^{\circ}C$ )	$\Delta H_{m,PLA}$ (J/g)
pure PLA			61.5	107.7	30.4	170.1	35.5
PLA/DDBH-0.1			61.6	102.9	31.8	169.5	40.8
PLA/DDBH-0.3	94.3	19.4	61.7	96.4	4.0	169.4	42.5
PLA/DDBH-0.5	115.3	39.4	61.9			167.8	43.3
PLA/DDBH-0.7	122.3	42.0	62.1			166.8	46.4
PLA/DDBH-0.9	122.4	42.4	62.0			166.7	46.6

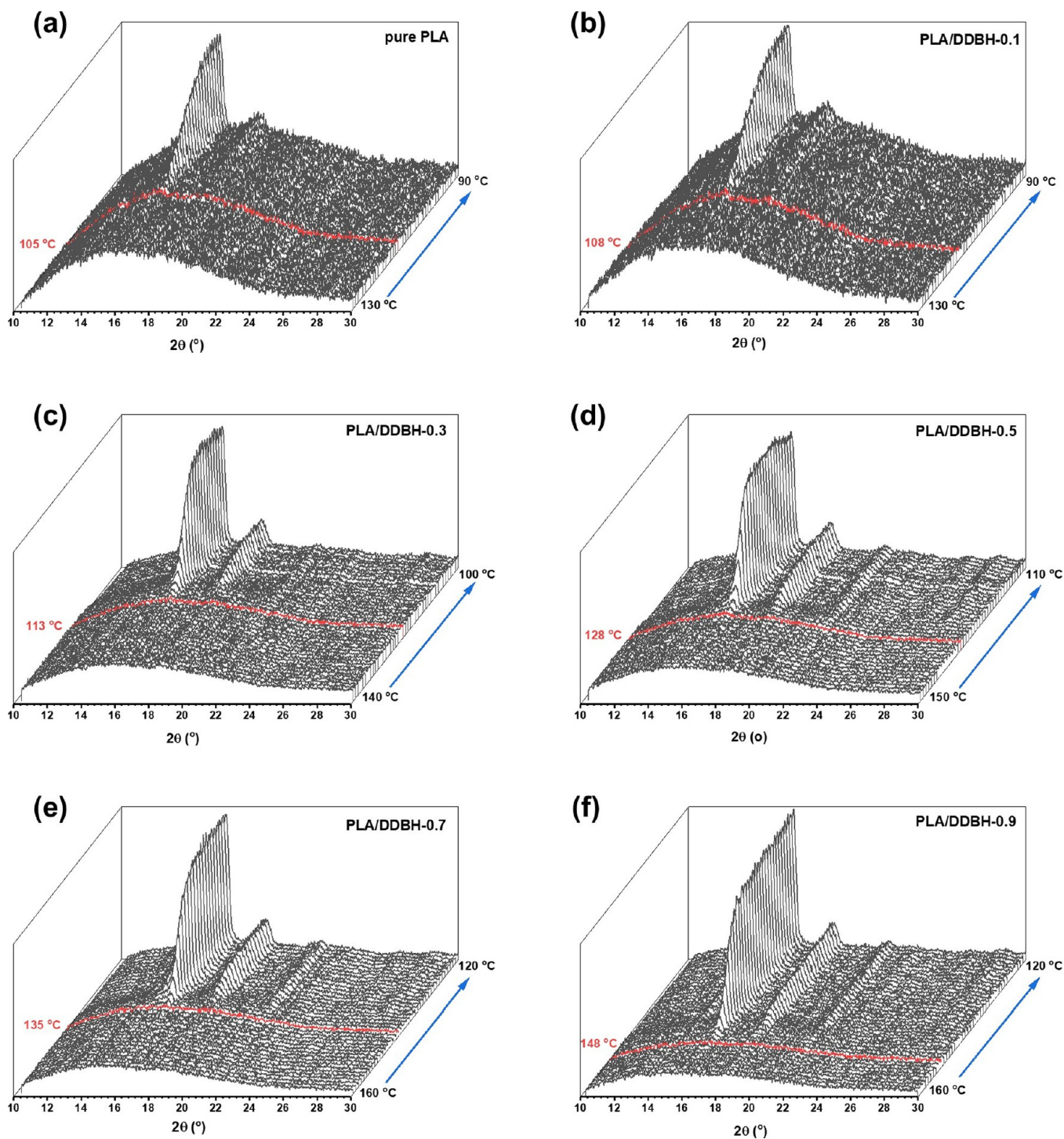
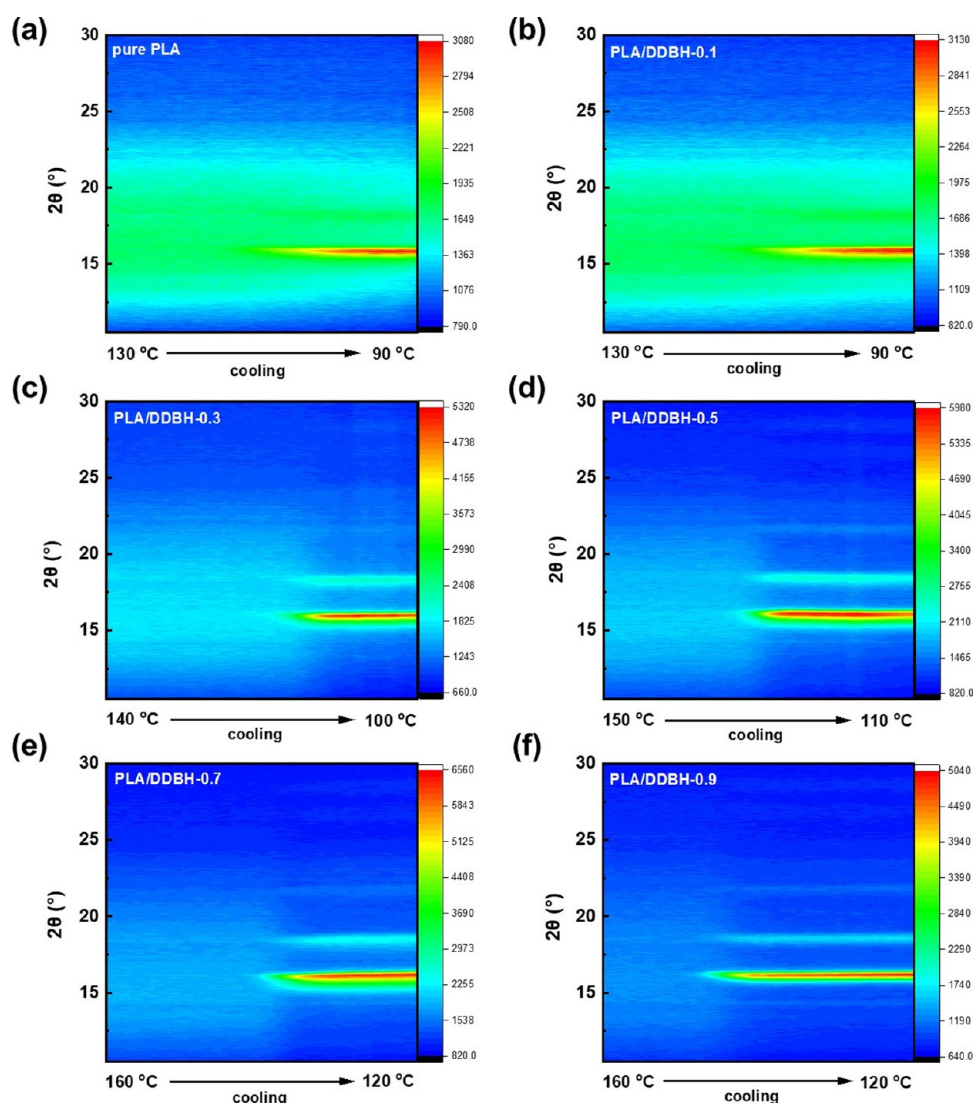


Figure 8. In situ WAXD profiles for pure PLA (a) and PLA/DDBH blends (b–f).



**Figure 9.** Contour plots of the in situ WAXD pattern for pure PLA (a) and PLA/DDBH blends (b–f).

concentration range of 0.5–0.9 wt %, DDBH recrystallized into dendrite-like structures during the isothermal crystallization process and the crystal morphology for PLA was changed from a spherical crystal to a similar dendritic crystal (Figure 4d–f). Moreover, a shorter period is needed for the PLA crystal to emerge in its blends (0.5–0.9 wt % DDBH) during the isothermal crystallization. These findings indicated that the crystallization rate of PLA was significantly improved by DDBH and the crystalline morphology of PLA was greatly changed due to the addition of DDBH.

Owing to the very fast crystallization rate of PLA/DDBH-0.9 blend during the isothermal crystallization process at 130 °C, dendrite-like structures formed during the isothermal crystallization at 150 °C were observed (Figure 5). It was interesting to find that in the PLA/DDBH-0.9 blend, DDBH formed dendrite-like structures during the isothermal crystallization process, with enhancement in a degree of branching. Further, PLA crystal was attached to the dendrite-like structures for crystallization. The scheme for self-assembly of DDBH and crystallization of PLA/DDBH blend is shown in Figure 6.

**3.2. Crystallization Behaviors of Pure PLA and PLA/DDBH Blends.** The crystallization behaviors of pure PLA and PLA/DDBH blends were investigated by nonisothermal

crystallization and isothermal crystallization kinetics. Figure 7 shows the nonisothermal crystallization curves of pure PLA and PLA/DDBH blends, and the data are presented in Table 2. Apparently, the incorporation of DDBH had an influence on the crystallization of PLA in the PLA/DDBH blends. During the second heating run, the cold crystallization temperature ( $T_{cc,PLA}$ ) of PLA appeared in pure PLA, PLA/DDBH-0.1, and PLA/DDBH-0.3 blends. On adding 0.3 wt % DDBH,  $T_{cc,PLA}$  decreased from 107.7 (pure PLA) to 96.4 °C. Moreover, when the concentration of DDBH was more than 0.1 wt %, PLA/DDBH blends showed crystallization temperatures ( $T_{c,PLA}$ ) of PLA during the first cooling run. As the DDBH content was increased,  $T_{c,PLA}$  in blends increased from 94.3 °C (PLA/DDBH-0.3) to 122.4 °C (PLA/DDBH-0.9). The nonisothermal crystallization curves of pure PLA and PLA/DDBH blends showed similar trends at different cooling rates (Figure S2). On the one hand,  $T_{c,PLA}$  clearly shifted to a higher temperature range along with a decrease in the cooling rates of pure PLA and its blends. A lower cooling rate could provide sufficient time to nucleate, due to which crystallization could occur at a higher temperature. On the other hand,  $T_{c,PLA}$  in the blends was higher than that of pure PLA for any given cooling rate. The shifting of  $T_{c,PLA}$  to a higher temperature range

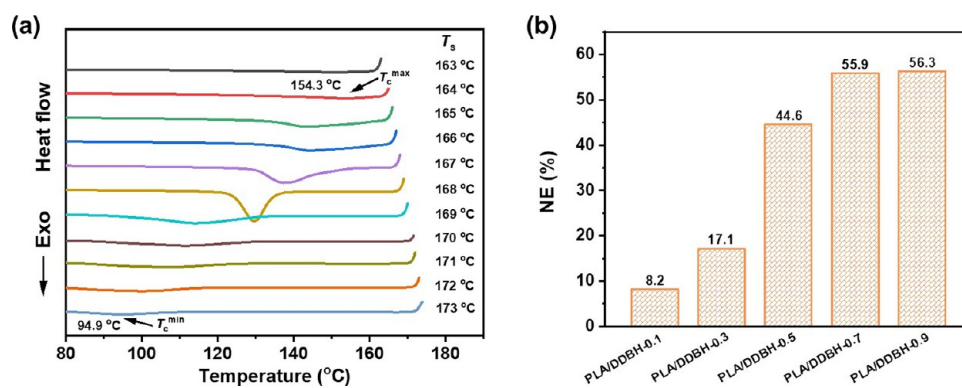


**Figure 10.** (a) DSC curves of pure PLA after self-nucleation at different self-nucleation temperatures ( $T_s$ ) and (b) NE of the DDBH for PLA/DDBH blends.

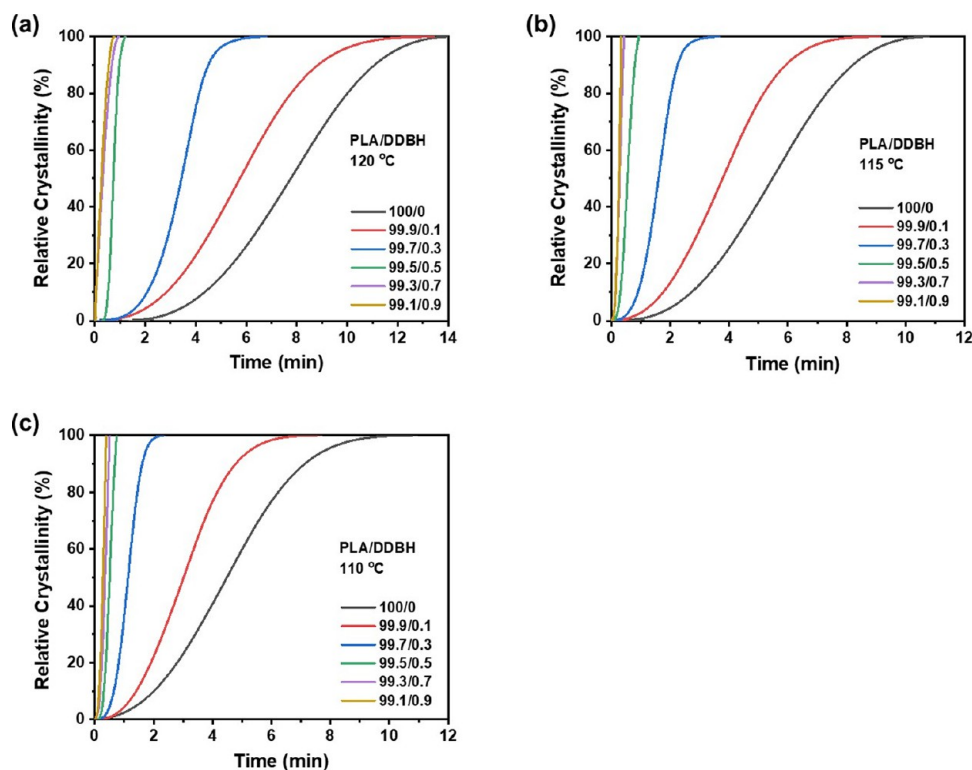


**Figure 11.** Variation of relative crystallinity with crystallization time for pure PLA and PLA/DDBH blends at various crystallization temperatures: (a) 120 °C, (b) 115 °C, and (c) 110 °C.

indicated an improvement in the crystallization ability of PLA by DDBH. Meanwhile, the melting temperature ( $T_{m,PLA}$ ) for PLA reduced from 170.1 (pure PLA) to 166.7 °C (PLA/DDBH-0.9). In addition, the melting enthalpy ( $\Delta H_{m,PLA}$ ) of PLA increased as the DDBH concentration was increased.

The nonisothermal crystallization behaviors of pure PLA and PLA/DDBH blends were further investigated by in situ WAXD analysis by studying the changes in the ordered structures of neat PLA and PLA/DDBH blends when cooled from 200 to 50 °C (Figure 8). For pure PLA (Figure 8a), as the temperature decreased to 90 °C, two diffraction peaks for  $\alpha$ -crystal appeared at around 16.7° and 19.1°, which corresponded to the (200)/(110) and (203) lattice planes of PLA, respectively.<sup>42</sup> The characteristic diffraction peaks of the  $\alpha$  form appeared when the temperature was below 105 °C. Further, the intensity of  $\alpha$ -characteristic peaks increased continuously from 105 to 90 °C. Similar diffraction peaks of

the  $\alpha$ -form of PLA appeared at 108 °C for the PLA/DDBH-0.1 blend (Figure 8b). With an increase in DDBH content, the intensities of characteristic diffraction peaks of the  $\alpha$  form of crystalline PLA increased. When the concentration of DDBH was between 0.1 and 0.9 wt %, three diffraction peaks of  $\alpha$ -crystal appeared at around 16.7°, 19.1°, 22.0°, corresponding to the (200)/(110), (203), (210) lattice planes of PLA, respectively (Figure 8c–e).<sup>42</sup> The PLA/DDBH-0.9 blend (Figure 8f) showed four typical diffraction peaks of the  $\alpha$  form of crystalline PLA at 14.8°, 16.7°, 19.1°, 22.0°, corresponding to (010), (200)/(110), (203), (210) lattice planes of PLA, respectively.<sup>42</sup> This indicated that the crystallinity increased with the DDBH concentration increased. Moreover, the temperature at which the diffraction peaks characteristic of  $\alpha$  form appeared in the PLA samples (0.3, 0.5, 0.7, or 0.9 wt % DDBH), increased with an increase in DDBH content. For example, when the temperature reached 148 °C,

the characteristic diffraction peaks of crystalline PLA for the PLA/DDBH-0.9 blend appeared. These results implied that DDBH promoted the crystallization of PLA. The contour plots for the in situ WAXD patterns of PLA blends are shown in Figure 9. The integrated peak intensities corresponding to the  $\alpha$  form of PLA gradually increased until they reached the maximum when the testing temperature was decreased.

The nucleation efficiency (NE) of NA was evaluated using the following equation<sup>38</sup>:

$$NE(\%) = \frac{T_c - T_c^{\min}}{T_c^{\max} - T_c^{\min}} \times 100 \quad (1)$$

where  $T_c^{\min}$  is the minimum crystallization temperature when pure PLA is cooled from the molten state in the absence of self-nucleation,  $T_c^{\max}$  is the maximum crystallization temperature when the crystallized PLA is partially melted and self-nucleated with the remaining crystals, and  $T_c$  is the crystallization temperature of the PLA/DDBH blend at the same cooling rate. According to self-nucleation theory,<sup>43</sup>  $T_c^{\min}$  and  $T_c^{\max}$  of PLA are 94.9 and 154.3 °C, respectively (Figure 10a). Based on the  $T_c$  acquired from nonisothermal crystallization process during cooling at 5 °C/min (Table S1), the NE of DDBH was evaluated and illustrated in Figure 10b. The NE of 0.1 wt % DDBH was 8.2%, whereas that of 0.5 wt % DDBH was 44.6%. For PLA samples nucleated by 0.7 or 0.9 wt % DDBH, the NEs of DDBH were all above 50%, which indicated that the DDBH had high NE.

The overall kinetics of isothermal crystallization of pure PLA and PLA/DDBH blends were studied by DSC at different isothermal crystallization temperatures (Figures 11 and S3). The time-dependent relative crystallinity ( $X_t$ ) was evaluated using the equation<sup>44</sup>:

$$X_t = \frac{\Delta H_c(t)}{\Delta H_c(\infty)} = \frac{\int_0^t \frac{dH_c}{dt} dt}{\int_0^\infty \frac{dH_c}{dt} dt} \quad (2)$$

where  $dH_c/dt$  is the heat flow rate.

The Avrami equation was applied to the isothermal crystallization kinetics of pure PLA and PLA/DDBH blends<sup>45</sup>:

$$1 - X_t = \exp(-kt^n) \quad (3)$$

where  $n$  is the Avrami exponent and  $k$  is the crystallization rate constant.

The half-crystallization time ( $t_{1/2}$ ), defined as the time corresponding to 50%  $X_t$ , can be calculated by the following equation<sup>46</sup>:

$$t_{1/2} = \left( \frac{\ln 2}{k} \right)^{1/n} \quad (4)$$

The related kinetic parameters ( $n$ ,  $k$ , and  $t_{1/2}$ ) of isothermal crystallization of PLA and its blends are listed in Table 3. Values of  $n$  for pure PLA crystallized at 120, 115, and 110 °C were 2.34, 2.40, and 2.65, respectively. These values suggested that the spherulite growth of pure PLA was three-dimensional with athermal nucleation.<sup>11</sup> Meanwhile, all  $n$  values for PLA/DDBH blends were in the range of 2 to 3. These findings suggested that changes in the crystallization temperature and concentration of DDBH could not alter the crystallization mechanism of PLA.

Overall crystallization rate could be evaluated from values of  $t_{1/2}$ , wherein a lower  $t_{1/2}$  value corresponded to a higher

**Table 3. Isothermal Crystallization Kinetic Parameters for Pure PLA and PLA/DDBH Blends Are Based on the Avrami Equation**

samples	isothermal crystallization temperatures ( $T_c$ , °C)	crystallization kinetic parameters		
		$n$	$K$ ( $\text{min}^{-n}$ )	$t_{1/2}$ (min)
pure PLA	120	2.34	0.010	6.12
	115	2.40	0.016	4.83
	110	2.65	0.015	4.24
PLA/DDBH-0.1	120	2.56	0.011	5.14
	115	2.32	0.036	3.60
PLA/DDBH-0.3	110	2.64	0.036	3.08
	120	2.94	0.026	3.05
	115	2.89	0.187	1.57
PLA/DDBH-0.5	110	2.59	0.675	1.01
	120	2.95	4.478	0.53
	115	2.43	5.395	0.43
PLA/DDBH-0.7	110	2.93	9.445	0.40
	120	2.59	10.59	0.35
	115	2.46	17.96	0.27
PLA/DDBH-0.9	110	2.32	17.01	0.24
	120	2.39	14.69	0.28
	115	2.77	31.62	0.25
	110	2.30	25.10	0.22

crystallization rate. The  $t_{1/2}$  value decreased with a decrease in the isothermal crystallization temperatures for pure PLA and its blends (Table 3). This might be due to the observation that the investigation of isothermal melt crystallization of PLA in this study was a process controlled by nucleation because of the low supercooling process. Furthermore,  $t_{1/2}$  values of PLA/DDBH blends were smaller than that of pure PLA at any given crystallization temperature, suggesting that the overall crystallization rate of PLA improved with the addition of DDBH. Such as, the  $t_{1/2}$  value at 120 °C reduced from 6.12 min (pure PLA) to 0.28 min (PLA/DDBH-0.9 blend).

**3.3. X-ray and FT-IR Analyses.** WAXD patterns of the samples, which were preheated at 200 °C for 5 min and then cold-molded at 25 °C for 5 min, are shown in Figure 12a. Only a broad diffraction peak, assigned to the amorphous regions of PLA, was observed in the WAXD patterns of pure PLA. After the addition of DDBH, the characteristic diffraction peaks of crystalline PLA appeared. Moreover, the crystallinity ( $X_c$ ) of PLA in PLA/DDBH blend increased with an increase in DDBH content (Table 4).

The apparent crystal size ( $L_{hkl}$ ) was calculated by Scherrer's equation<sup>47–49</sup>:

$$L_{hkl} = \frac{K\lambda}{\beta_{hkl} \times \cos \theta} \quad (5)$$

$$\beta_{hkl} = \sqrt{B_{hkl}^2 - b^2} \quad (6)$$

where  $K$  is the Scherrer constant (0.89),  $\lambda$  is the wavelength of the X-rays (1.5418 Å),  $\theta$  is Bragg's angle,  $B$  is the half-width of the diffraction angle for (200)/(110) lattice plane, and  $b$  is the instrumental constant (0.1°). The values of  $L_{hkl}$  are presented in Table 4. It was evident that the crystallite dimensions of PLA/DDBH blends decreased with an increase in DDBH content. After blending with 0.9 wt % DDBH, the  $L_{hkl}$  value of (200)/(110) lattice plane of PLA decreased to 71.1 nm. The addition of DDBH to PLA/DDBH blends

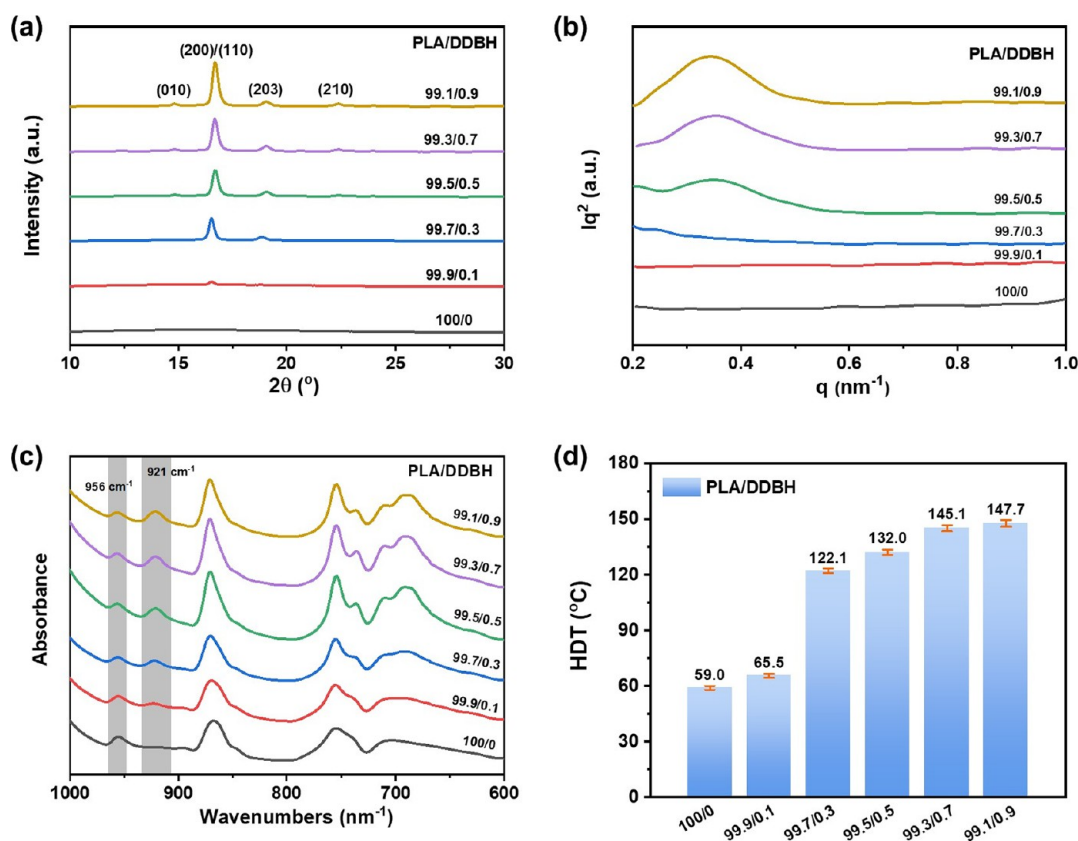


Figure 12. WAXD patterns (a), SAXS patterns (b), FT-IR spectra (c), and HDT (d) for pure PLA and PLA/DDBH blends.

Table 4. Crystallite Dimensions of Pure PLA and PLA/DDBH Samples Obtained from WAXD

samples	crystallinity ( $X_c$ , %)	$L_{hkl}$ (nm) (200)/(110)
pure PLA		
PLA/DDBH-0.1	2.5	
PLA/DDBH-0.3	28.3	81.8
PLA/DDBH-0.5	45.8	77.7
PLA/DDBH-0.7	50.6	75.7
PLA/DDBH-0.9	58.2	71.1

elevated the nucleating density of the crystal plate and decreased the size of the crystal plate.

SAXS was employed to investigate the crystal structure of pure PLA and its blends. Figure 12b presents SAXS data with Lorentz correction. In the case of pure PLA, PLA/DDBH-0.1, and PLA/DDBH-0.3 blends, the scattering intensity was too weak to be detected, which can be attributed to their lower crystallinity and relatively thinner and defective lamellae. The long period ( $d_{ac}$ ), defined as the thickness of the crystal layer along with one inter lamellar amorphous layer, was measured along the lamellar normal and calculated using Bragg's equation<sup>50</sup>:

$$d_{ac} = \frac{2\pi}{q_{max}} \quad (7)$$

where  $q_{max}$  is the maximum scattering intensity of the SAXS pattern at the  $q$  value.

The autocorrelation function  $K(z)$  could then be derived from the inverse Fourier transform of these two separated curves as follows<sup>51,52</sup>:

$$K(z) = \frac{\int_0^\infty I(q)\cos(qz)dq}{\int_0^\infty I(q)dq} \quad (8)$$

The thicknesses of the amorphous layer ( $d_a$ ) and crystalline lamella ( $d_c = d_{ac} - d_a$ ) can be obtained from the autocorrelation function (Figure S4 and Table 5).  $d_c$  of PLA

Table 5. Aggregation Structure Parameters of Pure PLA and PLA/DDBH Samples Were Obtained from SAXS

samples	$q_{max}$ (nm <sup>-1</sup> )	$d_{ac}$ (nm)	$d_a$ (nm)	$d_c$ (nm)
pure PLA				
PLA/DDBH-0.1				
PLA/DDBH-0.3				
PLA/DDBH-0.5	0.3508	17.91	2.01	15.90
PLA/DDBH-0.7	0.3536	17.77	1.62	16.15
PLA/DDBH-0.9	0.3423	18.36	1.43	16.93

for PLA/DDBH samples grew, whereas  $d_a$  of PLA decreased with an increase in DDBH concentration. The increase in thickness of crystalline lamellae implied an advancement in the crystallization of PLA blends enabled by DDBH.

The structural changes occurring at the molecular level in PLA, before and after the addition of DDBH, were studied with FT-IR (Figure 12c). The peak at 956 cm<sup>-1</sup> is assigned to the amorphous phase of PLA, whereas the peak at around 921 cm<sup>-1</sup> is assigned to the crystalline phase of PLA.<sup>53</sup> The peak for amorphous PLA could be seen in the FT-IR spectra of all of

the samples. Meanwhile, the peak for crystalline PLA could be seen in the PLA/DDBH blends. After the addition of DDBH, the changes in the 921 and 956  $\text{cm}^{-1}$  peaks were obvious. The intensity of the 921  $\text{cm}^{-1}$  peak increased, whereas the intensity of the 956  $\text{cm}^{-1}$  peak decreased with an increase in DDBH content. This meant that the crystallinity of PLA increased with an increase in the concentration of DDBH.

**3.4. Heat Resistance.** HDT of samples was tested to confirm their heat resistances (Figure 12d). The HDT of pure PLA was 59.0 °C. After incorporating 0.9 wt % DDBH, the HDT of PLA/DDBH-0.9 blend increased to 147.7 °C. It suggested that DDBH could effectively improve the heat resistance of PLA matrix. By increasing the crystallinity and the thickness of crystalline lamella of the polymer the heat resistance of polymers could be increased.<sup>54,55</sup> Therefore, the incorporation of DDBH led to an increase in  $X_c$  and  $d_c$  of PLA in the PLA/DDBH blend, which consequently increased its HDT. This indicated that the incorporation of DDBH improved the dimensional stability and decreased the thermal deformation of PLA.

## 4. CONCLUSIONS

In this work, DDBH was effectively used as NA with self-assembly properties to prepare PLA/DDBH blends by melt-blending. The formation of DDBH with different morphologies and sizes in the PLA melt was studied. In PLA/DDBH-0.5, PLA/DDBH-0.7, and PLA/DDBH-0.9 blends, DDBH recrystallized into a dendrite-like structure during the cooling process. POM analysis showed that during the isothermal crystallization process, the morphology of PLA crystal changed from spherical to dendritic crystal, due to the addition of DDBH. Combined results of DSC and in situ WAXD showed that the crystallization behaviors of PLA/DDBH blends were influenced by DDBH. In comparison with pure PLA,  $T_{cc}$  of PLA disappeared and  $T_c$  of PLA increased as DDBH concentration increased. Moreover, the DDBH had a high nucleation effect, wherein for the PLA/DDBH-0.9 blend, the NE of DDBH was 56.3%. The results of isothermal crystallization kinetics showed that the overall crystallization rate of PLA improved with the addition of DDBH. After blending with 0.9 wt % DDBH, the  $t_{1/2}$  value at 120 °C was shortened to 0.28 min. In addition, the incorporation of DDBH increased the crystallinity and crystalline lamellar thickness of PLA, whereas it decreased the apparent crystal size of PLA. Finally, compared to pure PLA, the heat resistances of PLA/DDBH blends were improved. The HDT increased from 59 (pure PLA) to 147.7 °C (PLA/DDBH-0.9 blend). Therefore, the incorporation of DDBH could overcome the disadvantages of PLA and significantly enhance the crystallization rate and heat distortion temperature of PLA. This means that the application of PLA was greatly extended.

## ■ ASSOCIATED CONTENT

### SI Supporting Information

The Supporting Information is available free of charge at <https://pubs.acs.org/doi/10.1021/acsomega.3c06384>.

Rheological properties of pure PLA and PLA/DDBH blends; crystallization properties of pure PLA and PLA/DDBH blends; POM micrographs of PLA/DDBH-3 and PLA/DDBH-5 blends; and WAXD patterns and FT-IR spectra of DDBH (PDF)

## ■ AUTHOR INFORMATION

### Corresponding Author

Yan Zhao – Key Laboratory of Polymer Ecomaterials, Changchun Institute of Applied Chemistry, Chinese Academy of Sciences, Changchun 130022, China; [orcid.org/0009-0003-3535-2962](https://orcid.org/0009-0003-3535-2962); Email: [zhaoyan@ciac.ac.cn](mailto:zhaoyan@ciac.ac.cn)

### Authors

Zhixiang Yan – Key Laboratory of Polymer Ecomaterials, Changchun Institute of Applied Chemistry, Chinese Academy of Sciences, Changchun 130022, China

Yanqin Huang – State Key Laboratory of Molecular Engineering of Polymers, Department of Macromolecular Science, Fudan University, Shanghai 200438, China

Wenfeng Zhao – State Key Laboratory of Molecular Engineering of Polymers, Department of Macromolecular Science, Fudan University, Shanghai 200438, China

Bin Wu – State Key Laboratory of Molecular Engineering of Polymers, Department of Macromolecular Science, Fudan University, Shanghai 200438, China

Chengkai Liu – Key Laboratory of Polymer Ecomaterials, Changchun Institute of Applied Chemistry, Chinese Academy of Sciences, Changchun 130022, China

Xiangyu Yan – Jilin COFCO Biochemical Technology Co. Ltd., Changchun 130033, China

Hongwei Pan – Key Laboratory of Polymer Ecomaterials, Changchun Institute of Applied Chemistry, Chinese Academy of Sciences, Changchun 130022, China; [orcid.org/0000-0003-3779-1718](https://orcid.org/0000-0003-3779-1718)

Huilang Zhang – Key Laboratory of Polymer Ecomaterials, Changchun Institute of Applied Chemistry, Chinese Academy of Sciences, Changchun 130022, China

Complete contact information is available at:

<https://pubs.acs.org/10.1021/acsomega.3c06384>

### Notes

The authors declare no competing financial interest.

## ■ ACKNOWLEDGMENTS

This work was supported by the Science & Technology Bureau of Jilin Province of China (20230201028GX).

## ■ REFERENCES

- (1) Chae, Y.; An, Y. J. Current research trends on plastic pollution and ecological impacts on the soil ecosystem: A review. *Environ. Pollut.* **2018**, *240*, 387–395.
- (2) Blasing, M.; Amelung, W. Plastics in soil: Analytical methods and possible sources. *Sci. Total Environ.* **2018**, *612*, 422–435.
- (3) Cross, R. A.; Kalra, B. Biodegradable polymers for the environment. *Science* **2002**, *297*, 803–807.
- (4) Scott, G. 'Green' polymers. *Polym. Degrad. Stab.* **2000**, *68*, 1–7.
- (5) Yu, L.; Dean, K.; Li, L. Polymer blends and composites from renewable resources. *Prog. Polym. Sci.* **2006**, *36*, 576–602.
- (6) Garlotta, D. A literature review of poly(lactic acid). *J. Polym. Environ.* **2001**, *9*, 63–84.
- (7) Nampoothiri, K. M.; Nair, N. R.; John, R. P. An overview of the recent developments in polylactide (PLA) research. *Bioresour. Technol.* **2010**, *101*, 8493–8501.
- (8) Inkinen, S.; Hakkarainen, M.; Albertsson, A. C.; Sodergard, A. From lactic acid to poly(lactic acid) (PLA): Characterization and analysis of PLA and its precursors. *Biomacromolecules* **2011**, *12*, 523–532.
- (9) Carrasco, F.; Pages, P.; Gamez-perez, J.; Santana, O. O.; Maspocho, M. L. Processing of poly(lactic acid): Characterization of

chemical structure, thermal stability and mechanical properties. *Polym. Degrad. Stab.* **2010**, *95*, 116–125.

(10) Rasal, R. M.; Janorkar, A. V.; Hirt, D. E. Poly(lactic acid) modifications. *Prog. Polym. Sci.* **2010**, *35*, 338–356.

(11) Saeidlou, S.; Huneault, M. A.; Li, H. B.; Park, C. B. Poly(lactic acid) crystallization. *Prog. Polym. Sci.* **2012**, *37*, 1657–1677.

(12) Lim, L. T.; Auras, R.; Rubino, M. Processing technologies for poly(lactic acid). *Prog. Polym. Sci.* **2008**, *33*, 820–852.

(13) Mikos, A. G.; Thorsen, A. J.; Czerwonka, L. A.; Bao, Y.; Langer, R.; Winslow, D. N.; Vacanti, J. P. Preparation and characterization of poly(L-lactic acid) foams. *Polymer* **1994**, *35*, 1068–1077.

(14) Kawai, T.; Rahman, N.; Matsuba, G.; Nishida, K.; Kanaya, T.; Nakano, M.; Okamoto, H.; Kawada, J.; Usuki, A.; Honma, N.; Nakajima, K.; Matsuda, M. Crystallization and melting behavior of poly(L-lactic acid). *Macromolecules* **2007**, *40*, 9463–9469.

(15) Li, H. B.; Huneault, M. A. Effect of nucleation and plasticization on the crystallization of poly(lactic acid). *Polymer* **2007**, *48*, 6855–6866.

(16) Feng, Y. Q.; Ma, P. M.; Xu, P. W.; Wang, R. Y.; Dong, W. F.; Chen, M. Q.; Joziassse, C. The crystallization behavior of poly(lactic acid) with different types of nucleating agents. *Int. J. Biol. Macromol.* **2018**, *106*, 955–962.

(17) Xie, J. Y.; Gu, K.; Zhao, Y.; Yao, J. R.; Chen, X.; Shao, Z. Z. Enhancement of the mechanical properties of poly(lactic acid)/epoxidized soybean oil blends by the addition of 3-aminophenylboronic acid. *ACS Omega* **2022**, *7*, 17841–17848.

(18) Han, L. J.; Han, C. Y.; Bian, J. J.; Bian, Y. J.; Lin, H. J.; Wang, X. M.; Zhang, H. L.; Dong, L. S. Preparation and characteristics of a novel nano-sized calcium carbonate (nano-CaCO<sub>3</sub>)-supported nucleating agent of poly(L-lactide). *Polym. Eng. Sci.* **2012**, *52*, 1474–1484.

(19) Zhao, Y.; Wei, B. L.; Wu, M.; Zhang, H. L.; Yao, J. R.; Chen, X.; Shao, Z. Z. Preparation and characterization of antibacterial poly(lactic acid) nanocomposites with N-halamine modified silica. *Int. J. Biol. Macromol.* **2020**, *155*, 1468–1477.

(20) Zhao, H. W.; Bian, Y. J.; Li, Y.; Han, C. Y.; Dong, Q. L.; Dong, L. S.; Gao, Y. Enhancing cold crystallization of poly(L-lactide) by a montmorillonitic substrate favoring nucleation. *Thermochim. Acta* **2014**, *588*, 47–56.

(21) Li, Y.; Han, C. Y.; Yu, Y. C.; Xiao, L. G.; Shao, Y. Effect of content and particle size of talc on nonisothermal melt crystallization behavior of poly(L-lactide). *J. Therm. Anal. Calorim.* **2019**, *135*, 2049–2058.

(22) Qin, C. Y.; Chen, K.; Xu, R. Y.; Wang, Y. M. Nucleating effect of boron nitride nanotubes on poly(lactic acid) crystallization. *Colloid Polym. Sci.* **2022**, *300*, 775–784.

(23) Zhao, Q.; Wang, B. W.; Qin, C. Y.; Li, Q. X.; Liu, C. T.; Shen, C. Y.; Wang, Y. M. Nonisothermal melt and cold crystallization behaviors of biodegradable poly(lactic acid)/Ti<sub>3</sub>C<sub>2</sub>T<sub>x</sub> MXene nanocomposites. *J. Therm. Anal. Calorim.* **2022**, *147*, 2239–2251.

(24) Guo, X. Y.; Luo, C. Y.; Fang, M. G.; Sun, J. X.; Chen, M. Y. Effects of self-assembled nucleating agent on the crystallization behavior, thermal properties, and mechanical properties of polylactic acid. *J. Appl. Polym. Sci.* **2023**, *140*, No. e54222.

(25) Xu, T.; Zhang, A. J.; Zhao, Y. Q.; Han, Z.; Xue, L. X. Crystallization kinetics and morphology of biodegradable poly(lactic acid) with a hydrazide nucleating agent. *Polym. Test.* **2015**, *45*, 101–106.

(26) Wang, L.; Wang, Y. N.; Huang, Z. G.; Weng, Y. X. Heat resistance, crystallization behavior, and mechanical properties of polylactide/nucleating agent composites. *Mater. Des.* **2015**, *66*, 7–15.

(27) Gui, Z. Y.; Lu, C.; Cheng, S. J. Comparison of the effects of commercial nucleation agents on the crystallization and melting behaviour of polylactide. *Polym. Test.* **2013**, *32*, 15–21.

(28) Aliotta, L.; Cinelli, P.; Coltelli, M. B.; Righetti, M. C.; Gazzano, M.; Lazzeri, A. Effect of nucleating agents on crystallinity and properties of poly(lactic acid) (PLA). *Eur. Polym. J.* **2017**, *93*, 822–832.

(29) Aliotta, L.; Sciara, L. M.; Cinelli, P.; Canesi, I.; Lazzeri, A. Improvement of the PLA crystallinity and heat distortion temperature optimizing the content of nucleating agents and the injection molding cycle time. *Polymers* **2022**, *14*, 977.

(30) Nagarajan, V.; Mohanty, A. K.; Misra, M. Crystallization behavior and morphology of polylactic acid (PLA) with aromatic sulfonate derivative. *J. Appl. Polym. Sci.* **2016**, *133*, 43673.

(31) Fortunati, E.; Armentano, I.; Zhou, Q.; Puglia, D.; Terenzi, A.; Berglund, L. A.; Kenny, J. M. Microstructure and nonisothermal cold crystallization of PLA composites based on silver nanoparticles and nanocrystalline cellulose. *Polym. Degrad. Stab.* **2012**, *97*, 2027–2036.

(32) Byun, Y.; Rodriguez, K.; Han, J. H.; Kim, Y. T. Improved thermal stability of polylactic acid (PLA) composite film via PLA- $\beta$ -cyclodextrin-inclusion complex systems. *Int. J. Biol. Macromol.* **2015**, *81*, 591–598.

(33) Ikada, Y.; Jamshidi, K.; Tsuji, H.; Hyon, S. H. Stereocomplex formation between enantiomeric poly(lactides). *Macromolecules* **1987**, *20*, 904–906.

(34) Wang, Z. G.; Wang, X. H.; Hsiao, B. S.; Andjelic, S.; Jamiolkowski, D.; Mcdivitt, J.; Fischer, J.; Zhou, J.; Han, C. C. Time-resolved isothermal crystallization of absorbable PGA-co-PLA copolymer by synchrotron small-angle X-ray scattering and wide-angle X-ray diffraction. *Polymer* **2001**, *42*, 8965–8973.

(35) Zhao, X. P.; Yu, J. J.; Xinyu liang, X. Y.; Huang, Z. P.; Li, J. C.; Peng, S. X. Crystallization behaviors regulations and mechanical performances enhancement approaches of polylactic acid (PLA) biodegradable materials modified by organic nucleating agents. *Int. J. Biol. Macromol.* **2023**, *233*, No. 123581.

(36) Yue, Y.; Sha, X.; Wang, F. S.; Gao, Y.; Zhang, L. L.; Zhu, Y. G.; Wang, X. X.; Feng, J. C. Non-negligible effect of additives in the application of successive self-nucleation and annealing fractionation for microstructure characterization of matrix resin in additive-containing samples. *ACS Appl. Polym. Mater.* **2021**, *3*, 4634–4644.

(37) Nagarajan, V.; Zhang, K. Y.; Misra, M.; Mohanty, A. K. Overcoming the fundamental challenges in improving the impact strength and crystallinity of PLA biocomposites: influence of nucleating agent and mold temperature. *ACS Appl. Mater. Interfaces* **2015**, *7*, 11203–11214.

(38) Fillon, B.; Lotz, B.; Thierry, A.; Wittmann, J. C. Self-nucleation and enhanced nucleation of polymers. Definition of a convenient calorimetric efficiency scale and evaluation of nucleating additives in isotactic polypropylene ( $\alpha$  phase). *J. Polym. Sci., Polym. Phys.* **1993**, *31*, 1395–1405.

(39) Yue, Y.; Yi, J. J.; Wang, L.; Feng, J. C. Toward a more comprehensive understanding on the structure evolution and assembly formation of a bisamide nucleating agent in polypropylene melt. *Macromolecules* **2020**, *53*, 4381–4394.

(40) Luo, F.; Geng, C.; Wang, K.; Deng, H.; Chen, F.; Fu, Q.; Na, B. New understanding in tuning toughness of  $\beta$ -polypropylene: The role of  $\beta$ -nucleated crystalline morphology. *Macromolecules* **2009**, *42*, 9325–9331.

(41) Balzano, L.; Portale, G.; Peters, G. W. M.; Rastogi, S. Thermoreversible DMDBS phase separation in iPP: The effects of flow on the morphology. *Macromolecules* **2008**, *41*, 5350–5355.

(42) Pan, P. J.; Inoue, Y. Polymorphism and isomorphism in biodegradable polyesters. *Prog. Polym. Sci.* **2009**, *34*, 605–640.

(43) Schmidt, S. C.; Hillmyer, M. A. Polylactide stereocomplex crystallites as nucleating agents for isotactic polylactide. *J. Polym. Sci., Polym. Phys.* **2001**, *39*, 300–313.

(44) Avrami, M. Kinetics of phase change. I. General theory. *J. Chem. Phys.* **1939**, *7*, 1103–1112.

(45) Avrami, M. Kinetics of phase change. II. Transformation-time relations for random distribution of nuclei. *J. Chem. Phys.* **1940**, *8*, 212–224.

(46) Avrami, M. Granulation, phase Change, and microstructure kinetics of phase change. III. *J. Chem. Phys.* **1941**, *9*, 177–184.

(47) Zhang, L. N.; Ruan, D.; Zhou, J. P. Structure and properties of regenerated cellulose films prepared from cotton linters in NaOH/Urea aqueous solution. *Ind. Eng. Chem. Res.* **2001**, *40*, 5923–5928.

(48) Aghjeh, M. R.; Kazerouni, Y.; Otadi, M.; Khonakdar, H. A.; Jafari, S. H.; Ebadi-dehaghani, H.; Mousavi, S. H. A combined experimental and theoretical approach to quantitative assessment of microstructure in PLA/PP/Organo-Clay nanocomposites; wide-angle x-ray scattering and rheological analysis. *Composites, Part B* **2018**, *137*, 235–246.

(49) He, K.; Chen, N. F.; Wang, C. J.; Wei, L. S.; Chen, J. K. Method for determining crystal grain size by X-Ray diffraction. *Cryst. Res. Technol.* **2018**, *53*, No. 1700157.

(50) Tsuji, H.; Ikarashi, K.; Fukuda, N.; Poly(L-lactide): xii. Formation, growth, and morphology of crystalline residues as extended-chain crystallites through hydrolysis of poly(L-lactide) films in phosphate-buffered solution. *Polym. Degrad. Stab.* **2004**, *84*, 515–523.

(51) Strobl, G. R.; Schneider, M. J.; Voigtmartin, I. G. Model of partial crystallization and melting derived from small-angle X-ray scattering and electron microscopic studies on low-density polyethylene. *J. Polym. Sci., Polym. Phys.* **1980**, *18*, 1361–1381.

(52) Strobl, G. R.; Schneider, M. Direct evaluation of the electron density correlation function of partially crystalline polymers. *J. Polym. Sci., Polym. Phys.* **1980**, *18*, 1343–1359.

(53) Jia, S. L.; Han, L. J.; Chen, Y. J.; Pan, H. W.; Wang, X. Y.; Zhang, H. L.; Dong, L. S.; Zhang, H. X. Effect of initial crystallization on microstructure and mechanical properties of uniaxially pre-stretched poly(L-lactic acid). *Polymer* **2022**, *255*, No. 125143.

(54) Zhao, T.; Yu, J. S.; Pan, H. W.; Zhao, Y.; Zhang, Q. X.; Yu, X. Y.; Bian, J. J.; Han, L. J.; Zhang, H. L. Super-tough polylactic acid (PLA)/poly(butylene succinate) (PBS) materials prepared through reactive blending with epoxy-functionalized PMMA-GMA copolymer. *Int. J. Biol. Macromol.* **2023**, *251*, No. 126150.

(55) Deng, L.; Xu, C.; Wang, X. H.; Wang, Z. G. Supertoughened polylactide binary blend with high heat deflection temperature achieved by thermal annealing above the glass transition temperature. *ACS Sustain. Chem. Eng.* **2018**, *6*, 480–490.